Article

Chinese Science Bulletin

Condensed Matter Physics

July 2012 Vol.57 No.20: 2554–2561
doi: 10.1007/s11434-012-5205-0

Shock wave compression of poled $Pb_{0.99}[(Zr_{0.90}Sn_{0.10})_{0.96}Ti_{0.04}]_{0.98}Nb_{0.02}O_3$ ceramics: Depoling currents in axial and normal modes

JIANG DongDong[1,2,3*], DU JinMei[1], GU Yan[1] & FENG YuJun[2,3]

[1] *National Key Laboratory of Shock Wave and Detonation Physics, Institute of Fluid Physics, China Academy of Engineering Physics, Mianyang 621900, China;*
[2] *Electronic Materials Research Laboratory, Xi'an Jiaotong University, Xi'an 710049, China;*
[3] *International Center for Dielectric Research, Xi'an Jiaotong University, Xi'an 710049, China*

Received November 25, 2011; accepted February 24, 2012; published online May 22, 2012

We used a 100-mm diameter gas gun to investigate the output currents due to the sudden depolarization of poled $Pb_{0.99}[(Zr_{0.90}Sn_{0.10})_{0.96}Ti_{0.04}]_{0.98}Nb_{0.02}O_3$ ceramics under shock wave compression. We conducted shock wave experiments for the normal/axial mode with the polarization vector perpendicular/antiparallel to the shock vector. The shock pressure was in the range of 0.23 to 4.50 GPa. We measured the depoling currents under short-circuit, high-impedance, and breakdown conditions. Under the short-circuit condition, the dependence of the released charge on the shock pressure demonstrates the evolution of the ferroelectric-to-antiferroelectric phase transition. The onset pressure of the phase transition is between 0.23 and 0.61 GPa, and phase transition occurs completely above 1.22 GPa. The increasing load resistance decreases the released charge and increases the released energy. The results indicate that $Pb_{0.99}[(Zr_{0.90}Sn_{0.10})_{0.96}Ti_{0.04}]_{0.98}Nb_{0.02}O_3$ ceramic is a good candidate for a pulsed power generator.

shock wave, ferroelectric, antiferroelectric, phase transition

Citation: Jiang D D, Du J M, Gu Y, et al. Shock wave compression of poled $Pb_{0.99}[(Zr_{0.90}Sn_{0.10})_{0.96}Ti_{0.04}]_{0.98}Nb_{0.02}O_3$ ceramics: Depoling currents in axial and normal modes. Chin Sci Bull, 2012, 57: 2554–2561, doi: 10.1007/s11434-012-5205-0

Lead zirconate stannate titanate ceramic ($Pb(Zr,Sn,Ti)O_3$) is an important family of ferroelectrics and is usually modified by niobium (Nb) or lanthanum (La) to tailor its properties [1–7]. In particular, compositions close to the phase boundary of the ferroelectric (FE) and antiferroelectric (AFE) have attracted considerable interest for many years. Near the FE/AFE phase boundary, the free energy difference between the FE and AFE phase is very small, indicating that the FE/AFE phase transition can occur easily with an applied electric field or pressure [8,9]. These phase transitions are usually accompanied by a volume expansion/contraction [1,8], a development/release of electrical polarization [9], or an incommensurate modulation in structure [2–4,10], having many engineering applications. For instance, the longitudinal strain associated with the electric-field-enforced AFE-to-FE phase transition in $(Pb_{0.97}La_{0.02})(Zr_{0.66}Ti_{0.11}Sn_{0.23})O_3$ ceramics is up to 0.8%, which is useful in high-strain actuators [11].

On the other hand, the depolarization associated with the FE-to-AFE phase transition induced by a pressure is useful in converting mechanical to electrical energy. In the past, extensive investigations were conducted under quasi-static conditions such as hydrostatic [12,13] and uniaxial compression [14]. Berlincourt et al. [12,13] originally studied the loss of polarization in Nb-doped $Pb(Zr,Sn,Ti)O_3$ ceramics under hydrostatic loading. Fritz and Keck [15] developed the hydrostatic pressure-temperature phase diagram of $Pb_{0.99}Nb_{0.02}[(Zr_{0.86}Sn_{0.14})_{0.95}Ti_{0.05}]_{0.98}O_3$ ceramics. Afterwards, many studies have been conducted to characterize the effects of temperature and electric field on the FE-to-AFE phase transition under hydrostatic loading [16,17]. The above mentioned investigations indicate that $Pb(Zr,Sn,Ti)O_3$ ce-

*Corresponding author (email: jiangdongeast@163.com)

ramic, whose composition is near the FE/AFE phase boundary, is one of the main candidates for energy-conversion materials.

However, because of the slowly applied pressure in quasi-static experiments, the output electric power is usually too low to be used. The output power strongly depends on the method of applying the stress [18]. One method to overcome the problem is shock-wave loading. Compared with quasi-static loading, the shock wave is a useful tool to observe the dynamics of materials because it generates rapid change in pressure [19]. Sudden depolarization in ferroelectric ceramics through shock-wave compression was first proposed as a source of pulsed power more than 40 years ago [20]. Unsurprisingly, the dynamic behaviors of Pb(Zr,Sn,Ti)O_3 ceramics under shock wave compression have attracted considerate attention. Recently, Hugoniot states in the pressure range from 1.54 to 7.64 GPa in unpoled $Pb_{0.993}(Zr_{0.802}Ti_{0.049})Sn_{0.133}Nb_{0.016}O_3$ ceramics were investigated [21]. However, the significant lack of systematic study on the depolarization of poled Pb(Zr,Sn,Ti)O_3 ceramics has become the main obstacle preventing successful development of a pulsed power generator.

In this study, we investigate the output currents due to depolarization in $Pb_{0.99}[(Zr_{0.90}Sn_{0.10})_{0.96}Ti_{0.04}]_{0.98}Nb_{0.02}O_3$ ceramics under shock wave compression in axial and normal modes. We also discuss the effects of shock pressure and load resistance on the current, released charge, and energy.

1 Experimental procedure

1.1 Sample

Reagent-grade powders of Pb_3O_4 (>99%, ShuDu Powders Co. Ltd., Chengdu, China), ZrO_2, SnO_2, and TiO_2 (>99%, GuoYao Co. Ltd., Shanghai, China) were used to prepare the Pb(Zr,Sn,Ti)O_3 specimens with a FE/AFE-phase-boundary composition of $Pb[(Zr_{0.90}Sn_{0.10})_{0.96}Ti_{0.04}]O_3$. We added Nb_2O_5 powder (>99%, ZhuZhou Harden Alloys Co. Ltd., Zhuzhou, China) as a dopant. The final composition of the doped specimen was $Pb_{0.99}[(Zr_{0.90}Sn_{0.10})_{0.96}Ti_{0.04}]_{0.98}Nb_{0.02}O_3$ (PZST). This composition was in the low-temperature rhombohedral ferroelectric (F_{RLT}) phase and was near the phase boundary of the antiferroelectric orthorhombic (A_O) phase and F_{RLT} phase.

The powders were mixed by milling using zirconia balls (Tosoh Ceramics, Tokyo, Japan) and ethanol (>99.7%, HongYan chemical reagent Co. Ltd., Tianjin, China) as media. The powder mixture was calcined at 900°C for 2 h. The calcined powders were ball-milled one more time to crush agglometrates and then were pressed into cylinders (35 mm in diameter and 12 mm in height) in a steel die under a uniaxial pressure of 200 MPa for 5 min. Samples were sintered at 1250°C for 2 h in a lead-oxide-rich environment to minimize the lead-oxide volatilization. Then, samples were sliced and coated with silver electrodes. The silver paste was fired at 600°C. At last, the specimens were poled in silicone oil at 100°C by applying a dc electric field of 3 kV/mm for 5 min. After the temperature was lowered to 30°C, the dc electric field was removed. The piezoelectric constant d_{33} was measured using a d_{33} meter (Model ZJ-3D, Institute of Acoustics, Beijing, China). The average d_{33} was 68.0 pC/N. The density of the sintered ceramics was determined by the Archimedes method to be 7.80 g/cm^3. The hysteresis loop was measured using a ferroelectric test system (TF Analyzer 2000, aixACCT, Aachen, Germany). The remanent polarization (P_r) and low-frequency coercive field (E_c) (at 1 Hz) were 28.0 μC/cm^2 and 1.0 kV/mm, respectively. Figure 1 shows the released charge per unit area with the hydrostatic pressure. The F_{RLT}-to-A_O phase transition is marked by the sudden depolarization. The released charge is up to 28.2 μC/cm^2, which is in reasonable agreement with the remanent polarization. In addition, the threshold pressure of the phase transition, defined as the pressure at which half of the polarization is released, is approximately 140 MPa.

1.2 Shock-wave experiment

Figure 2 shows a schematic of the shock-wave experiments used to investigate the depolarization of the PZST ceramics. A 2024 aluminium (Al 2024) projectile body was accelerated by a 100-mm-diameter gas gun and impacted onto the polymethyl methacrylate (PMMA) target facing. The impact of the projectile facing (Al 2024/PMMA) onto the target facing initiated a shock wave propagating into the PZST ceramics. The velocity of the projectile, u_0, was measured by recording the time interval between the velocity pins in the vicinity of the target facing. The error was approximately 0.2%.

According to the relative orientation of the remanent polarization vector and the shock propagation vector, experiments were conducted with the normal mode (the polarization vector being perpendicular to the shock vector, Figure 3(a)) and axial mode (the polarization vector being antiparallel to

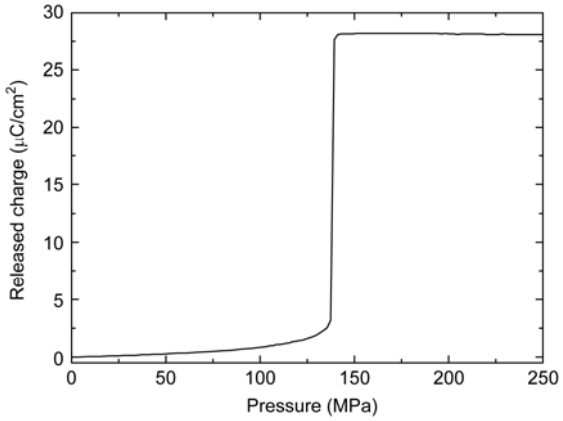

Figure 1 Hydrostatic-pressure-induced depolarization of poled $Pb_{0.99}[(Zr_{0.90}Sn_{0.10})_{0.96}Ti_{0.04}]_{0.98}Nb_{0.02}O_3$ ceramic.

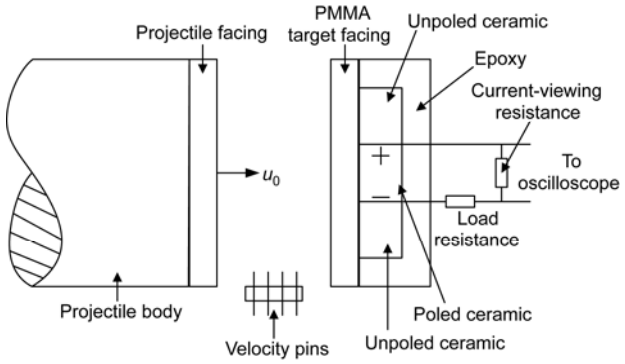

Figure 2 Schematic of the experimental arrangement used to study the depoling currents from the shock-loaded $Pb_{0.99}[(Zr_{0.90}Sn_{0.10})_{0.96}Ti_{0.04}]_{0.98}$-$Nb_{0.02}O_3$ ceramics.

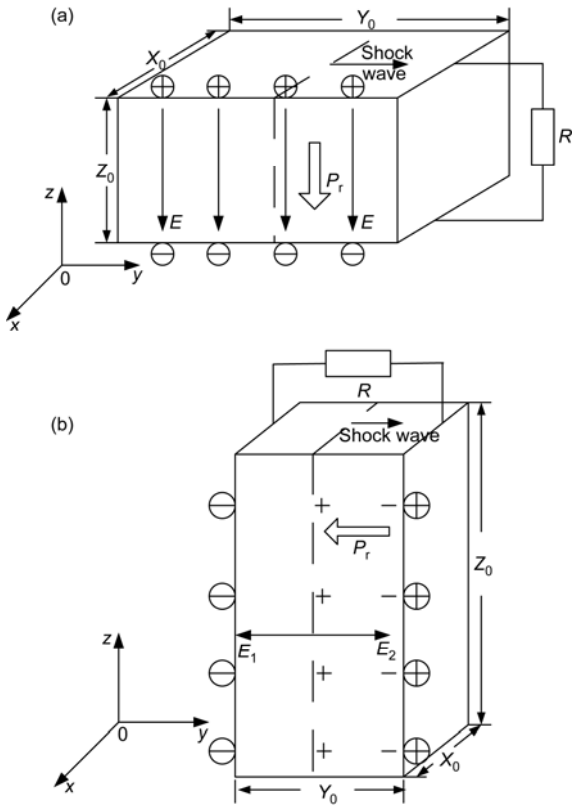

Figure 3 Schematic for the shock depoling of a $Pb_{0.99}[(Zr_{0.90}Sn_{0.10})_{0.96}$-$Ti_{0.04}]_{0.98}Nb_{0.02}O_3$ ceramic in the normal mode (a) and axial mode (b). P_r is the remanent polarization vector. The shock front at time t is indicated by the dashed line. As the shock wave passes through and depolarizes the ceramic, bound surface charge is released. The directions of the electric field E and polarization P_r for the two models are shown.

the shock vector, Figure 3(b)). For the normal mode, the dimensions of the ceramics were $X_0 \times Y_0 \times Z_0$=30.0 mm×10.0 mm×2.0 mm. Electrodes were deposited on the $X_0 \times Y_0$ faces. For the axial mode, the dimensions were $X_0 \times Y_0 \times Z_0$=20.0 mm×5.0 mm×10.0 mm. Electrodes were deposited on the $X_0 \times Z_0$ faces. To approach a uniaxial strain state, two pieces of unpoled ceramics sandwiched the poled ceramic. All ceramics were encapsulated with epoxy resin to reduce the probability of high-voltage electrical breakdown around their edges.

As the shock wave passed through the PZST ceramics, the compressed ceramic underwent the F_{RLT}-to-A_O phase transition and the polarization was released. The released charge flowed through the external circuit and generated the depoling current. The external circuit, which connected the electrodes of the ceramics, consisted of a low-inductance load resistance (R) and a low-inductance current-viewing resistance (r). In all experiments, r was 1.0 Ω and the voltage appearing for r was transmitted by a coaxial cable to an oscilloscope for recording. R was not used under the short-circuit condition. Under the high-impedance condition, R was put into transformer oil to prevent electrical breakdown.

A series of ten shock wave experiments were performed. Table 1 lists the impact facing, impact velocity, shock pressure, and load resistances for each experiment. The shock pressure was calculated with an impedance-match method dependent on the Hugoniot relations of the Al 2024 [22], PMMA [23] and PZST ceramic [24].

2 Results and discussion

2.1 Depoling current in normal-mode

The electric field between the electrodes is zero under the short-circuit condition (Figure 3(a), R=0). Therefore, the electric behavior is only dominated by the shock pressure. Figure 4 shows the depoling currents as a function of the shock pressure for the normal mode. The current magnitude is relatively small at 0.23 GPa, showing that the F_{RLT}-to-A_O phase transition does not occur. As the shock pressure increases from 0.61 to 2.47 GPa, the magnitude increases and reaches 22.2, 26.5, 30.3, 31.4 and 33.7 A.

Figure 5(a)–(e) show the depoling currents at 0.61, 1.03, 1.22, 2.47, and 4.50 GPa as a function of the load resistance. A strong electric field is generated between electrodes under the high-impedance condition. For instance, the peak electric field is up to 3.4 kV/mm at 2.47 GPa with a 200-Ω load resistance. Under the strong electric field, the capacitance (C) of the ceramic requires that part of the released charge remain on the electrodes rather than pass through the resistive load. Thus, comparing with the short-circuit cases, the currents with the resistive load increase gradually with the "RC" time constant. At the low shock pressure, i.e. 0.61 and 1.03 GPa, the eventual current amplitude under the short-circuit condition is higher than that at high impedance. Based on the soft mode theory for the FE-to-AFE phase transition, the electric field tends to stabilize the FE phase region and retard the FE-to-AFE phase transition [16]. Thus, the strong electric field may suppress the F_{RLT}-to-A_O phase transition, resulting in the decreasing magnitude at high impedance (Figure 5(a) and (b)). However, the high-impedance current eventually reaches the short-circuit value at 1.22,

Table 1 Experimental conditions for shock wave experiments

No.	Impact facing	Impact velocity (m/s)	Shock pressure (GPa)	Mode	Load resistance[a] (Ω)			
1	Al 2024	49.6	0.23	normal	none	200		
2	Al 2024	124.2	0.61	normal	none	200	300	
3	PMMA	260.3	0.81	axial	none	500		
4	Al 2024	200.6	1.03	normal	none	150	250	
5	PMMA	327.0	1.05	axial	none			
6	Al 2024	232.3	1.22	normal	none	300		
7	PMMA	473.0	1.60	axial	none			
				normal	none			
8	Al 2024	424.0	2.47	normal	none	200		
9	PMMA	718.6	2.67	axial	none	200	500	1000
				normal	none	1500		
10	PMMA	1073.4	4.50	axial	none	500		
				normal	none	300	1500	2000

a) None represents the short-circuit case.

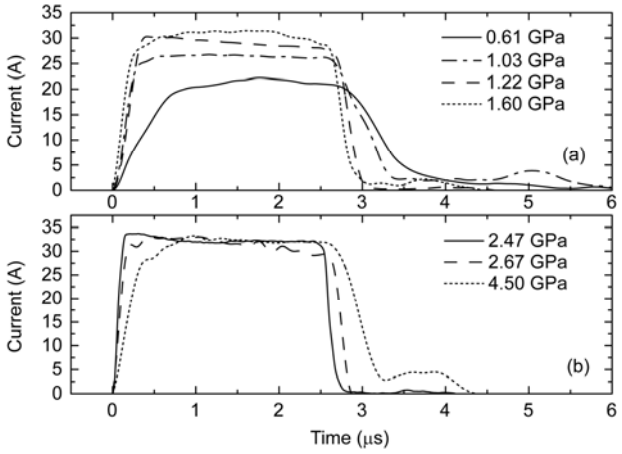

Figure 4 The depoling currents as a function of the shock pressure under the short-circuit condition for the normal mode in $Pb_{0.99}[(Zr_{0.90}Sn_{0.10})_{0.96}Ti_{0.04}]_{0.98}Nb_{0.02}O_3$ ceramics. (a) 0.61, 1.03, 1.22 and 1.60 GPa; (b) 2.47, 2.67 and 4.50 GPa.

2.47 and 4.50 GPa, showing that the electric field does not appear to have a significant effect on the current at high pressure. Insulation is a critical aspect and an interesting research topic in the technology of pulsed power. As we see in Figure 5(f), the breakdown currents show an abrupt decrease in amplitude before the shock wave has propagated through the ceramics. After breakdown, the currents fall to zero instantaneously.

2.2 Depoling current for the axial mode

Figure 6(a) shows the short-circuit current as a function of the shock pressure for the axial mode. The depoling currents are significantly different from those in Figure 4. The magnitude and time (t_0) at which the current reaches the peak value are very important for explaining the results. The magnitude and t_0 appear to be shock-pressure-dependent. At 0.81 GPa, the peak current is 20.9 A and appears at 1.35 μs. As the shock pressure increases, the peak shifts toward earlier times and increases in magnitude, i.e. at 1.60 GPa the maximum current is 48.2 A and appears at 0.94 μs. However, with further increase in shock pressure the current decreases in magnitude. For example, the peak value is 13.8 and 10.8 A at 2.67 and 4.50 GPa, respectively. Figure 6(b)–(d) depict the depoling currents as a function of the load resistance for the axial mode.

It should be noted that strong electrical fields are generated in axial mode under the short-circuit condition (Figure 3(b), R=0). Figure 3(b) is a schematic depicting the shock depoling a PZST ceramic. Prior to the passage of a shock wave through a short-circuit PZST ceramic, the bound surface charge neutralizes the polarization charge. Thus, the macroscopic electric field inside the ferroelectric is zero. As a shock wave passes through the sample and reduces the P_r of the compressed ceramic, large fields are induced. The electric fields E_1 and E_2 are directed away from the shock front. Under the short-circuit condition, the electric fields E_1 and E_2 are related through the Kirchoff equation:

$$E_1 Ut = E_2\left(Y_0 - Ut\right), \quad 0 \leqslant t \leqslant \tau, \tag{1}$$

where U is the velocity of the shock wave and $\tau = Y_0/U$ is the shock transit time. The electric field E_1 and E_2 have been analyzed by developing a mathematical model [25]. The electric field E_2 is directed opposite to the polarization of the uncompressed ceramic. To some extent, the field E_2 can electrically depolarize the uncompressed ceramic prior to its shock compression. Thus, the PZST ceramics are simultaneously depolarized by the shock wave in the compressed region and by the electric field in the uncompressed region.

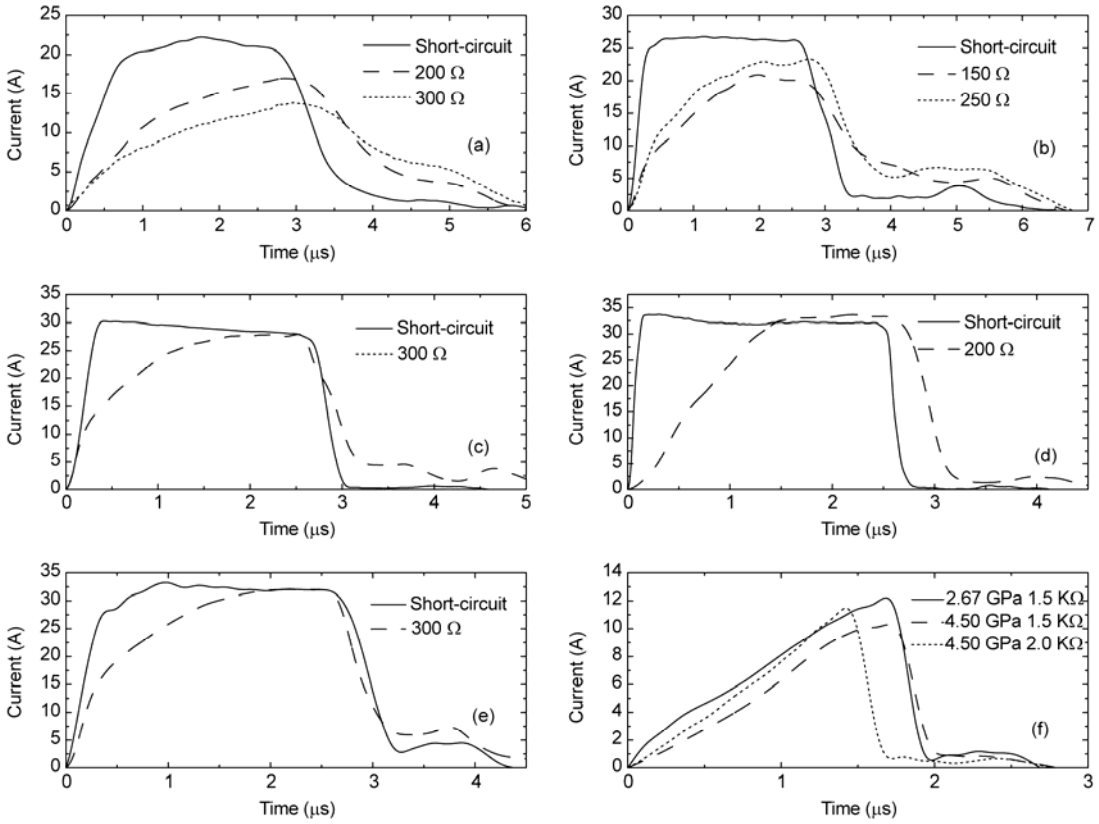

Figure 5 The depoling currents as a function of the load resistance at 0.61 GPa (a), 1.03 GPa (b), 1.22 GPa (c), 2.47 GPa (d), 4.50 GPa (e), and the breakdown currents for the normal mode (f).

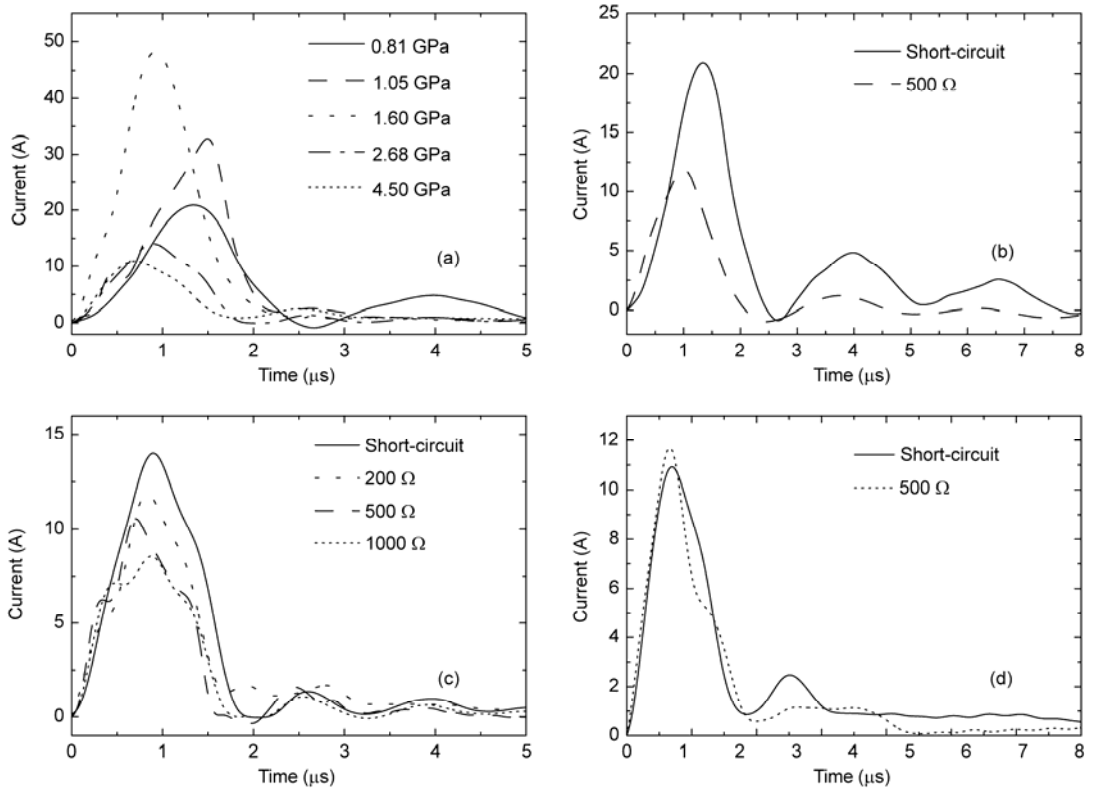

Figure 6 (a) The depoling currents under the short-circuit condition as a function of shock pressure for the axial mode; the depoling currents as a function of load resistance at 0.81 GPa (b), 2.67 GPa (c), and 4.50 GPa (d) for the axial mode.

2.3 Released charge

The normalized released charge (NRC) is given by

$$q = \int_0^{+\infty} I\mathrm{d}t \Big/ P_r A. \quad (2)$$

Here, I is the depoling current and A is the area of the electrode. Figure 7(a) shows the dependence of the NRC on the shock pressure for the normal mode under the short-circuit condition. The data for $Pb_{0.99}(Zr_{0.95}Ti_{0.05})_{0.98}Nb_{0.02}O_3$ (PZT 95/5-2Nb) ceramics are shown for comparison [26–28]. We should bear in mind that the shock wave promotes the FE-to-AFE phase transition. The dependence of the NRC on the shock pressure demonstrates the evolution of the F_{RLT}-to-A_O phase transition. For PZST ceramics, the onset of the phase transition is between 0.23 and 0.61 GPa. Between 0.61 and 1.22 GPa, the NRC increases with the shock pressure, indicating that the fraction of the PZST ceramics experiencing the phase transition increases. Above 1.22 GPa, the NRC is close to 1, indicating that the released charge matches the remanent polarization. Using the criterion of complete liberation of polarization as indicating complete phase transition, the phase transition is complete above 1.22 GPa. After the phase transition is complete, the NRC is insensitive to the shock pressure. Similar results are also observed for the PZT 95/5-2Nb ceramics [26–28].

Figure 7(b) shows the NRC for PZST ceramics as a function of the shock pressure for the axial mode under the short-circuit condition. The data for PZT 95/5-2Nb, $Pb_{0.99}Nb_{0.02}(Zr_{0.68}Ti_{0.07}Sn_{0.25})_{0.98}O_3$ (PSZT 68/7) and $Pb(Zr_{0.56}Ti_{0.44})O_3$ are shown for comparison [25,29]. For PZST ceramics, the NRC also appears to be dependent on the shock pressure. Maximum NRC is 0.93 at 1.60 GPa. At 0.81 and 1.05 GPa, incomplete phase transition accounts for the lower released charge. However, the released charge drops suddenly at 2.67 and 4.50 GPa. The charge decrease with increasing shock pressure, which was also observed in PZT 95/5-2Nb and PSZT 68/7 ceramics, can be attributed to the shock-induced conductivity. Halpin [30] calculated the resistivity of the shocked PZT 95/5-2Nb ceramics for the axial mode, and the value was on the order of 100 Ω cm in the range of 2.5 to 3.5 GPa.

Figure 8 plots the NRC as a function of the load resistance and of the shock amplitude in the region 0.61–4.50 GPa. At 2.67 GPa, the load resistances used for the axial mode have been multiplied by a factor of 1/2. For comparison, the NRC for PZT 95/5-2Nb is also shown, and the load resistances for PZT 95/5-2Nb have been multiplied by a factor of 1/100. The load resistances are 2.95, 5.96, 8.9, 9.17, 12 and 15 kΩ in [27]. The decreased charge at higher resistances can be explained by the decreased dynamic resistivity of the shock-loaded ceramics [31] and/or the electric field suppressing the FE-to-AFE phase transition [28].

2.4 Released energy

The output energy is the key parameter for applying the pulsed power. The electric energy density (ω) is given by

$$\omega = \int_0^{+\infty} I^2 R\mathrm{d}t \Big/ V, \quad (3)$$

where $V=X_0\times Y_0\times Z_0$ is the volume of the ceramic. Figure 9

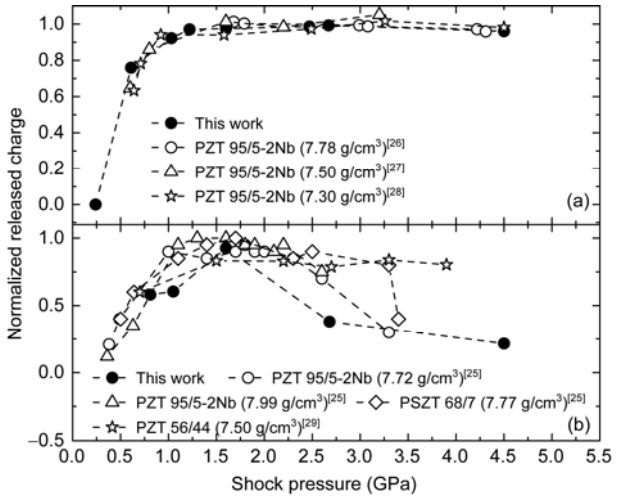

Figure 7 The dependence of the normalized released charge with respect to the P_r on shock pressure for normal mode (a) and axial mode (b). The error associated with each point is about ±1 μC or ±1.2%. In (a), the normalized P_r is 32.0 μC/cm^2 for PZT 95/5-2Nb ceramics (7.78 g/cm^3, [26]), 30.0 μC/cm^2 for porosity PZT 95/5-2Nb ceramic (7.55 g/cm^3, [27]; 7.30 g/cm^3, [28]). In (b), the normalized P_r is 33.5 μC/cm^2 for normally sintered PZT 95/5-2Nb (7.72 g/cm^3, [25]), 36.5 μC/cm^2 for hot-pressed PZT 95/5-2Nb (7.99 g/cm^3, [25]), 29.0 μC/cm^2 for normally sintered PSZT 68/7 (7.77 g/cm^3, [25]), and 31.0 μC/cm^2 for PZT 56/44 (7.50 g/cm^3, [29]).

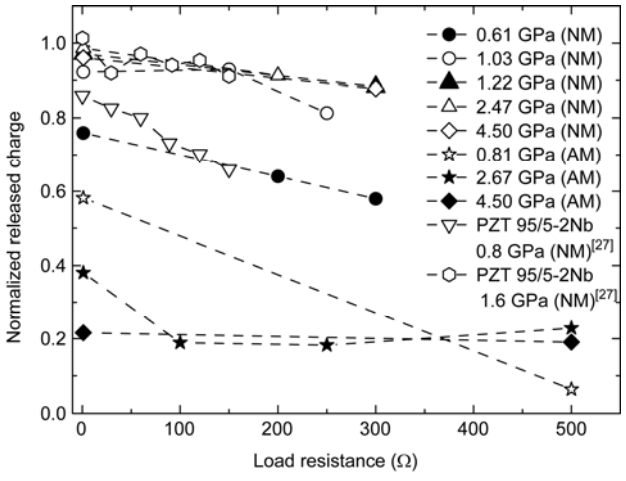

Figure 8 The normalized released charge as a function of shock pressure and load resistance for the normal mode (NM) and axial mode (AM). The error associated with each point is about ±1 μC or ±1.2%. For comparison, the released charge for PZT 95/5-2Nb ceramics is also shown, and the load resistances for PZT 95/5-2Nb have been multiplied by a factor of 1/100. The load resistances are 2.95, 5.96, 8.9, 9.17, 12 and 15 kΩ in [27]. The normalized P_r is 30.0 μC/cm^2 for PZT 95/5-2Nb ceramics (7.55 g/cm^3, [27]).

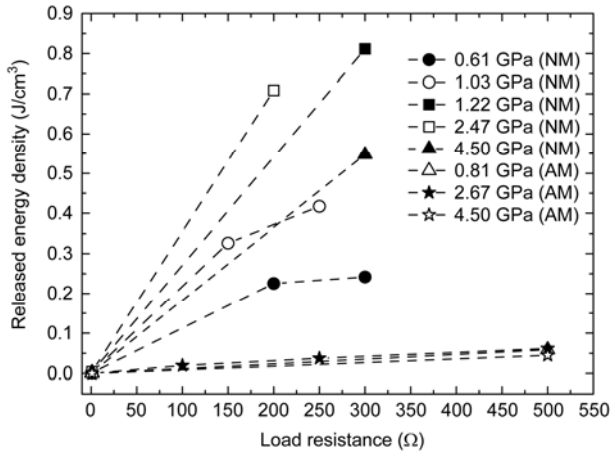

Figure 9 The dependence of the released energy density on the load resistance for the normal mode (NM) and axial mode (AM).

shows the plot of the released energy as a function of the load resistance. The released energy is close to zero under the short-circuit condition and increases with the load resistance at the same shock pressure. The maximum value is 0.81 J/cm^3 at 1.22 GPa with a 300-Ω load resistance for the normal mode. It is expected to obtain more electric energy when pulsed power is applied. The released energy for the normal mode is significantly higher than that for the axial mode, showing that the normal mode is more suitable for the pulsed power generator.

3 Conclusions

We investigated the depoling currents of poled $Pb_{0.99}[(Zr_{0.90}Sn_{0.10})_{0.96}Ti_{0.04}]_{0.98}Nb_{0.02}O_3$ ceramics under shock wave compression with axial and normal modes. We obtained the output currents under short-circuit, high-impedance, and breakdown conditions. The dependence of the released charge and energy on the shock pressure and load resistance was consistent with those of other ferroelectric ceramics. Based on these findings, we believe that $Pb_{0.99}[(Zr_{0.90}Sn_{0.10})_{0.96}Ti_{0.04}]_{0.98}Nb_{0.02}O_3$ ceramic is a good candidate material for pulsed power generators. Various ferroelectric and antiferroelectric phases have been reported in $Pb(Zr,Sn,Ti)O_3$ ceramics. Our work may provide a new recipe for designing pulsed power generators by searching for a suitable composition in the $Pb(Zr,Sn,Ti)O_3$ system.

This work was supported by the Science and Technology Foundation of China Academy of Engineering Physics (*2010A0201005*) *and the National Natural Science Foundation of China* (*10875095 and 50632030*).

1 Tan X, Frederick J, Ma C, et al. Can an electric field induce an antiferroelectric phase out of a ferroelectric phase? Phys Rev Lett, 2010, 105: 255702
2 He H, Tan X. *In situ* transmission electron microscopy study of the electric field-induced transformation of incommensurate modulations in a Sn-modified lead zirconate titanate ceramic. Appl Phys Lett, 2004, 85: 3187–3189
3 He H, Tan X. Electric field-induced transformation of incommensurate modulations in antiferroelectric $Pb_{0.99}Nb_{0.02}[(Zr_{1-x}Sn_x)_{1-y}Ti_y]_{0.98}O_3$. Phys Rev B, 2005, 72: 024102
4 He H, Tan X. Raman spectroscopy study of the phase transitions in $Pb_{0.99}Nb_{0.02}[(Zr_{0.57}Sn_{0.43})_{1-y}Ti_y]_{0.98}O_3$ ceramics. J Phys: Condens Matter, 2007, 19: 136003
5 Tan X, Jo W, Granzow T, et al. Auxetic behavior under electrical loads in an induced ferroelectric phase. Appl Phys Lett, 2009, 94: 042909
6 Tan X, Frederick J, Ma C, et al. Electric-field-induced antiferroelectric to ferroelectric phase transition in mechanically confined $Pb_{0.99}Nb_{0.02}[(Zr_{0.57}Sn_{0.43})_{0.94}Ti_{0.06}]_{0.98}O_3$. Phys Rev B, 2010, 81: 014103
7 Frederick J, Tan X, Jo W. Strains and polarization during antiferroelectric-ferroelectric phase switching in $Pb_{0.99}Nb_{0.02}[(Zr_{0.57}Sn_{0.43})_{1-y}Ti_y]_{0.98}O_3$ ceramics. J Am Ceram Soc, 2011, 94: 1149–1155
8 Pan W, Zhang Q, Bhalla A, et al. Field-forced antiferroelectric-to-ferroelectric switching in modified lead zirconate titanate stannate ceramics. J Am Ceram Soc, 1989, 72: 571–578
9 Xu Z, Feng Y J, Zheng S G, et al. Phase transition and dielectric properties of La-doped $Pb(Zr,Sn,Ti)O_3$ antiferroelectric ceramics under hydrostatic pressure and temperature. J Appl Phys, 2002, 92: 2663–2667
10 Viehland D, Forst D, Xu Z, et al. Incommensurately modulated polar structures in antiferroelectric Sn-modified lead zirconate titanate the modulated structure and its influences on electrically-induced polarizations and strains. J Am Ceram Soc, 1995, 78: 2101–2112
11 Pan W Y, Dam C Q, Zhang Q M, et al. Large displacement transducers based on electric field forced phase transitions in the tetragonal $(Pb_{0.97}La_{0.02})(Ti,Zr,Sn)O_3$ family of ceramics. J Appl Phys, 1989, 66: 6014–6023
12 Berlincourt D, Jaffe H, Krueger H H A, et al. Release of electric energy in $PbNb(Zr,Ti,Sn)O_3$. Appl Phys Lett, 1963, 3: 90–92
13 Berlincourt D, Krueger H H A, Jaffe B. Stability of phases in modified lead zirconate with variation in pressure, electric field, temperature and composition. J Phys Chem Solids, 1964, 25: 659–674
14 Fritz I J. Stress effects in two modified lead zirconate titanate ferroelectric ceramics. J Appl Phys, 1979, 50: 5265–5271
15 Fritz I J, Keck J D. Pressure-temperature phase diagrams for several modified lead zirconate ceramics. J Phys Chem Solids, 1978, 39: 1163–1167
16 Yang P, Payne D A. The effect of external field symmetry on the antiferroelectric-ferroelectric phase transformation. J Appl Phys, 1996, 80: 4001–4005
17 Xu Z, Feng Y J, Zheng S G, et al. Phase transition and dielectric properties of La-doped $Pb(Zr,Sn,Ti)O_3$ antiferroelectric ceramics under hydrostatic pressure. Mater Sci Eng B, 2003, 99: 441–444
18 Xu C N, Akiyama M, Nonaka K, et al. Electrical power generation characteristics of PZT piezoelectric ceramics. IEEE transactions on ultrasonics, ferroelectrics, and frequency control, 1998, 45: 1065–1070
19 Kadau K, Germann T C, Lomdahl P S, et al. Microscopic view of structural phase transitions induced by shock waves. Science, 2002, 296: 1681–1684
20 Neilson F W. Effects of strong shocks in ferroelectric materials. Bull Am Phys Soc, 1957, 2: 302
21 Millett J C F, Bourne N K, Deas D. The response of two ferroelectric ceramics to one-dimensional shock loading. J Phys D: Appl Phys, 2007, 40: 2948–2953
22 Walsh J M, Rice M H, McQueen R G, et al. Shock-wave compressions of twenty-seven metals equations of state of metals. Phys Rev, 1957, 108: 196–216
23 Barker L M, Hollenbach R E. Shock-wave studies of PMMA, fused silica, and sapphire. J Appl Phys, 1970, 41: 4208–4226
24 Doran D G. Shock-wave compression of barium titanate and 95/5 lead zirconate titanate. J Appl Phys, 1968, 39: 40–47

25 Halpin W J. Current from a shock-loaded short-circuited ferroelectric ceramic disk. J Appl Phys, 1966, 37: 153–163
26 Liu Y S, Liu G M, Zhang F P, et al. Experimental study of the depoling property of PZT-95/5 ferroelectric ceramic under shock wave loading (in Chinese). Piezoelectr Acoustoopt, 2008, 30: 58–60
27 Lysne P C. Dielectric properties of shock-wave-compressed PZT 95/5. J Appl Phys, 1977, 48: 1020–1023
28 Setchell R E. Shock wave compression of the ferroelectric ceramic $Pb_{0.99}(Zr_{0.95}Ti_{0.05})_{0.98}Nb_{0.02}O_3$: Depoling currents. J Appl Phys, 2005, 97: 013507
29 Mock W Jr, Holt W H. Axial current mode shock depoling of PZT 56/44 ferroelectric ceramic disks. J Appl Phys, 1979, 50: 2740–2748
30 Halpin W J. Resistivity estimates for some shocked ferroelectrics. J Appl Phys, 1968, 39: 3821–3826
31 Lysne P C. Resistivity of shock-wave-compressed PZT 95/5. J Appl Phys, 1977, 48: 4565–4568